J. Biochem. **134**, 151–158 (2003)
DOI: 10.1093/jb/mvg123

Roles of Ser130 and Thr126 in Chloride Binding and Photocycle of *pharaonis* Halorhodopsin

Maki Sato[1], Takashi Kikukawa[2], Tsunehisa Araiso[2], Hirotaka Okita[3], Kazumi Shimono[3], Naoki Kamo[3], Makoto Demura[*,1] and Katsutoshi Nitta[1]

[1]Division of Biological Sciences, Graduate School of Science, Hokkaido University, 060-0810; [2]Center for Advanced Science and Technology, Hokkaido University, 001-0021; and [3]Graduate School of Pharmaceutical Sciences, Hokkaido University, Sapporo 060-0812

Received March 20, 2003; accepted May 14, 2003

***Pharaonis* halorhodopsin (*p*hR) is an inward light-driven chloride ion pump in *Natronobacterium pharaonis*. In order to clarify the roles of the Ser130^{phR} and Thr126^{phR} residues, which correspond to Ser115^{shR} and Thr111^{shR} of *salinarum* hR (*s*hR), with regard to their Cl^--binding affinity and the photocycle, the wild-type *p*hR, and S130 and T126 mutants were expressed in *Escherichia coli* cells. The photocycles of the wild-type *p*hR, and S130 and T126 mutants were investigated in the presence of 1 M NaCl. Based on results of kinetic analysis involving singular value decomposition and global fitting, typical photointermediates K, L and O were identified, and the kinetic constants of decay or formation varied depending on the mutant. The photocycle scheme was linear for the wild-type *p*hR, and S130C, S130T and T126V mutants. On the other hand, the S130A mutant showed a branched pathway between the L-hR and L-O steps. The present study revealed the following two facts with respect to the Ser130^{phR} residue: 1) The OH group of this residue is important for Cl^- ion binding next to the Schiff base nitrogen, and 2) replacement of an Ala residue, which is unable to form a hydrogen bond, results in a branched photocycle. The implication of this branching was discussed.**

Key words: chloride pump, halorhodopsin, mutation, *Natronobacterium pharaonis*, photocycle.

Abbreviations: bR, bacteriorhodopsin; DM, *n*-dodecyl β-D-maltopyranoside; FTIR, Fourier transform infrared; hR, halorhodopsin; MOPS, 2-morpholinopropanesulfonic acid; *p*hR, *pharaonis* hR; *s*hR, *salinarum* hR; SVD, singular value decomposition.

Halorhodopsin (hR) and bacteriorhodopsin (bR) are transmembrane, seven-helix retinal proteins in the membrane of the archaeal bacterium *Halobacterium salinarum*. These retinal proteins act as an inward-directed electrogenic light-driven chloride ion pump and an outward-directed proton pump, respectively. BR has become a model system for studying membrane protein structure, protein folding, bioenergetics, photochemistry, and mechanism of proton transport (*1–5*). Although detailed knowledge about the proton transport of bR has been accumulated, much less information is available on the molecular mechanism of Cl^- transport by hR, particularly with respect to site-specific mutagenesis.

The crystal structure of *salinarum* hR (*s*hR) was recently solved by X-ray diffraction (*6*) at 1.8 Å resolution. The structural similarity to *salinarum* bR (*s*bR) and *pharaonis* sensory rhodopsin II (phoborhodopsin) is highest for the pentahelical bundle C-G, resulting in root mean square deviation (rmsd) on the main chain Cα atoms of 0.74 Å for bR (*7*) and 0.89 Å for *pharaonis* sensory rhodopsin II (phoborhodopsin) (*8*), respectively. The crystal structure of *s*hR shows that a single Cl^- ion next to the Schiff base nitrogen is closely associated with the isomerizable chromophore (Fig. 1). Chloride accepts hydrogen bonds only from two-bound water (3.1 Å and 3.2 Å) and Oγ of Ser115^{shR} (3.1 Å), whereas Cγ of Thr111^{shR} is also closely associated with the Cl^- ion (3.6 Å). Therefore, Ser115^{shR} that is connected through hydrogen bonds to Cl^- in the ground state might be instrumental in keeping the chloride solvated in the internal cavity, although there has been no report on Ser115^{shR}-specific mutagenesis. On the other hand, a report of the modest effect of the T111V mutation of *s*hR on transport activity (*9*) suggests that the close contact of T111 with Cl^- is only an additional participant in the binding site (*6*).

Although many hRs have been identified and reported (*10–13*), only those from *Halobacterium salinarum* (*14*, *15*) and *Natronobacterium pharaonis* (*16–18*) have been extensively studied. At present, there is no report on the crystal structure of *pharaonis* hR (*p*hR). Since the primary structures of *s*hR and *p*hR are highly homologous (66%) (*19*), their tertiary structures would seem to be conserved. More recently, in order to clarify the role of the Ser130^{phR} residue of *Natronobacterium pharaonis* hR (*p*hR), which corresponds to Ser115^{shR} in *salinarum* hR, the wild-type *p*hR, and Ser130 mutants with Thr, Cys, and Ala substituted were expressed in *Escherichia coli* (*20*). The wild-type *p*hR and all mutants showed a blue-shift of the absorption maximum (λ_{max}) upon Cl^- addition, from which the dissociation constants of Cl^- were deter-

[*]To whom correspondence should be addressed. Tel: +81-11-706-2771, Fax: +81-11-706-2771, E-mail: demura@sci.hokudaia.ac.jp

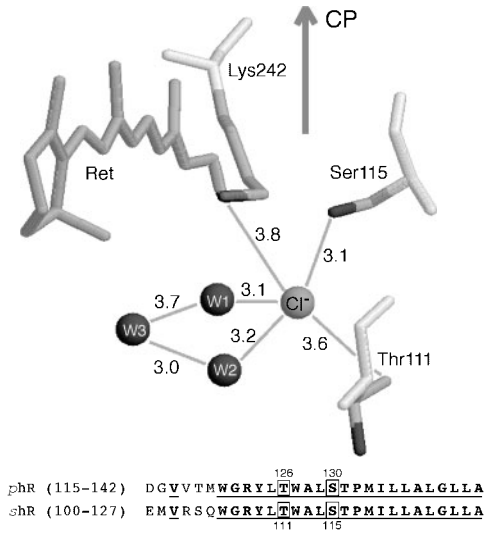

Fig. 1. **Chromophore structures of *s*hR.** The picture is based on PDB codes, 1E12. Ret denotes the all-*trans* retnylidene chromophores. Cl^-, W1, W2, and W3 indicate the chloride ion located in the binding site and three bound waters, respectively. Direction CP indicates the cytoplasmic side. Only three amino acids, Lys242, Ser115, and Thr111, which are close to the chloride binding site, are shown. Black sticks at the side chains of Ser115 and Thr111 indicate hydroxyl oxygens. The lower part of the figure indicates the homology in the helix C region between *p*hR and *s*hR.

mined. The dissociation constants were 5, 89, 153, and 159 mM for the wild-type *p*hR, and S130A, S130T, and S130C mutants, respectively, at pH 7.0 and 25°C, indicating that S130 of *p*hR is important for the chloride binding affinity. In addition, the Ser130 mutation affected the protein stability.

The photocycle of *p*hR includes intermediates analogous in the case of bR. Spectral and kinetic studies have clarified the following photocycle for *p*hR: hR → K ↔ L ↔ N ↔ O ↔ hR′ → hR (*16*). In the case of *H. salinarum* hR (*s*hR), the O-intermediate does not accumulate, presumably for kinetic reasons (*21*). The release and uptake of Cl^- are associated with the N to O and O to hR′ reactions, respectively. Mutagenesis studies on *s*hR have revealed that the extracellular pair R108/T111^{shR} plays an important role in the chloride uptake by increasing the affinity of this binding site, and the cytoplasmic pair R200/T203^{shR} is a candidate for the Cl^- binding site concerning the release (*9*). Furthermore, His-95^{shR}, which is located in the extracellular loop between helices B and C, is presumably an important residue for Cl^- uptake. The molecular basis of the switch event of hR and the origin of the difference in ion specificity from bR have not yet been determined. The chloride binding kinetics of blue *p*hR (*p*hR^{blue}), which has lost Cl^- near the chromophore, have been measured as time-resolved absorption changes in the dark with stopped-flow rapid mixing (*22*). The rate constant at 100 mM NaCl at 25°C was 260 s^{-1} with an apparent activation energy of 35 kJ/mol. These values were in good agreement with the process of Cl^- uptake in the photocycle (O → hR′ reaction) reported previously (*16*). In addition, the Cl^- concentration dependences of the two rates were similar. These observations suggested that the O-intermediate is similar to *p*hR^{blue} and that Cl^- uptake during the photocycle may be ruled by a passive process (*22*).

In this study, we expressed histidine-tagged wild-type *p*hR, and Thr126^{phR} and Ser130^{phR} point mutants, which correspond to Thr111^{shR} and Ser115^{shR}, in *E. coli* cells, and clarified the role of the Ser130^{phR} residue in the photocycle reactions. The results we obtained indicate that Ser130^{phR} in helix C is a more essential residue for chloride binding and transport/switch than Thr126^{phR} is. There are various advantages to using *p*hR, which has been reported to be more stable than *s*hR. Moreover, the retinal isomeric composition does not change because of light/dark adaptation (*18*), and *p*hR transports not only halide but also nitrate at about the same rate (*19*). In addition, *E. coli* expression of the archaeal retinal protein was recently reported by Shimono *et al*. (*23*). And finally, the use of a histidine-tagged protein makes it possible to purify *p*hR in only one step (*24*), thereby allowing simple and large-scale preparation (*20*, *22*).

MATERIALS AND METHODS

Construction of Expression Plasmids for T126 and S130 Mutants Having a Histidine Tag—Mutant plasmids for the expression of Thr126^{phR} and Ser130^{phR} mutants with Val (T126V) and Ala (S130A), and Cys (S130C) and Thr (S130T) substituted were constructed with a Quikchange Site-Directed Mutagenesis Kit (Stratagene Cloning Systems), and the modified pET-21c(+) vector to utilize the histidine-tagged region (*22*). The sequences of the primers designated to replace the Thr126 codon with another amino acid codon were 5′-GGC CGC TAT CTG GTG (for Val) TGG GCC CTT TCG-3′, 5′-CGA AAG GGC CCA CAC (for Val) CAG ATA GCG GCC-3′, and the Ser130 codon described in a previous report (*20*). We performed PCR with the following reagents (total reaction volume = 50 μl): (i) pET*p*hR-His 40 ng, (ii) primer 0.3 μM each, (iii) dNTP mixture 200 μM, (iv) *Pfu Turbo* DNA polymerase 2.5 units, and (v) 10× buffer (QuikChange Site-Directed Mutagenesis Kit). The standard PCR reaction cycling comprised 1 cycle of 95°C, 1 min; 16 cycles of 95°C, 0.5 min; 55°C, 1 min; and 68°C, 12 min; and finally 1 cycle of 95°C, 20 min. As the next stage, 40 μl of the PCR product was treated with 10 units *Dpn*I (37°C, 1 h), and then the transformation of *Epicurian coli* XL-1-Blue Supercompetent cells was performed with 2 μl of the reactant. The mutations introduced into the plasmid were confirmed by DNA sequencing using a DNA sequencing kit (Applied Biosystems, Foster City, CA), and each mutated plasmid was introduced into BL21(DE3) cells. Transformed cells were selected as to ampicillin resistance.

Protein Expression and Purification of phR—The protein expression and purification procedures for *E. coli* BL21(DE3) cells harboring the plasmid were described in detail in a previous paper (*22*). Fractions of the proteins separated with Ni-NTA agarose (Qiagen, Hilden, Germany) were collected by elution (flow rate, 56 ml/h) with buffer E (50 mM Tris-HCl, pH 7.0, 300 mM NaCl, 150 mM imidazole, and 0.1% *n*-dodecyl β-D-maltopyranoside (dodecylmaltoside, DM) (Dojindo Lab, Kumamoto).

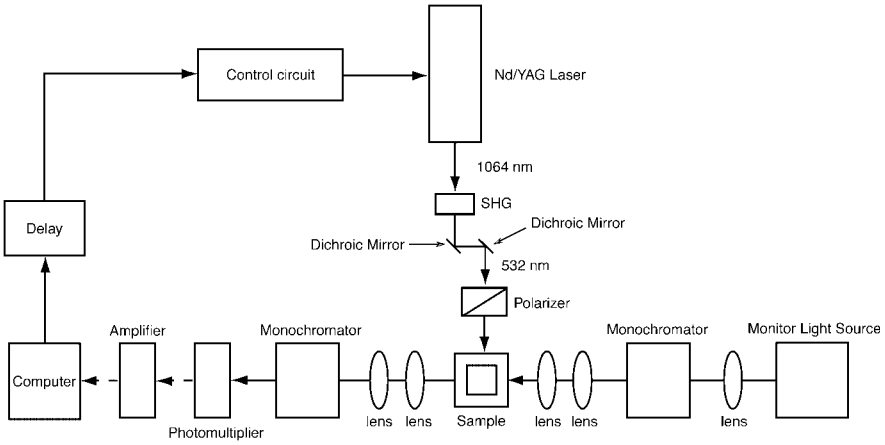

Fig. 2. **Block diagram of the flash photometer used for measurement of the absorption change with a Nd/YAG laser. SHG, second-harmonic generator.**

Preparation of Blue Species—Anion-depleted blue species of the wild-type *p*hR and mutants were prepared by replacing buffer E with buffer C (10 mM 2-morpholinopropanesulfonic acid, MOPS (pH 7.0) and 0.1% DM) by passage over Sephadex-G25 (1.25 × 20 cm; Amersham Pharmacia Biotech, Uppsala, Sweden) at the flow rate of 2 ml/min. After buffer exchange, the protein concentration was estimated using an excitation coefficient ε_{600} of 50,000 $M^{-1}\cdot cm^{-1}$ (*27*). The anion-depleted species of S130A and S130C were used immediately after preparation (within 5 h) to avoid denaturing.

Absorption Measurements—Visible absorption spectra (300–750 nm) of the wild-type *p*hR and mutants were measured with a Jasco J-725 spectropolarimeter (Jasco, Tokyo) as described in detail in a previous paper (*22*).

Flash Photolysis Spectroscopy—A computer-controlled flash-photolysis system (Fig. 2) was constructed as described in a previous paper (*25*). Samples were excited at 532 nm (7 ns pulse width, ~5 mJ/pulse, 1 Hz repetition rate) using the second harmonic of the fundamental beam of a Q-switched Nd-YAG laser (Surelite I-10; Continuum, Santa Clara, CA). The source of the monitoring light was a 150-W xenon arc lamp (C4251; Hamamatsu Photonics), and the beam of the monitoring light was perpendicular to that of the actinic flash. A photomultiplier (R2949; Hamamatsu Photonics) was used to detect the monitoring light passing through the sample cell (10 × 10-mm quartz cuvette). To select the measuring wavelength and to exclude the scattered actinic flash from the sample, we used two monochromators, one at the rear of the monitoring light source and the other in front of the photomultiplier. The output of the photomultiplier was amplified and stored in a computer equipped with an A/D converter (12-bit resolution, 0.8 μs per point). At each measuring wavelength (41 wavelengths, every 10 nm from 350 to 750 nm), the absorption change was obtained as the average of 50–100 data collection. The sample concentration was adjusted so that the absorbance at l_{max} in the visible region was about 0.5, and the temperature was kept at 20°C. The bleaching of the sample by the actinic flash was negligible.

Singular value decomposition (SVD) treatment (*26*) was performed to determine the number of spectral components, as well as to remove the noise. Kinetic analysis and global fitting were performed using the Igor Pro 3.14 software package (Wave Metrics, Lake Oswego, OR).

RESULTS

Titration of the Wild-Type phR and Mutants with Chloride and Visible Absorption Spectra—The chloride-dependent absorption shift of the wild-type *p*hR and S130 mutants has been analyzed in order to clarify the dissociation constants of Cl^- (*20*). In the absence of Cl^-, S130C exhibited the same absorption maximum, l_{max}, as the wild-type *p*hR, whereas S130A caused red shifts, and T126V and S130T caused blue shifts of 11–12 nm (Table 1). The absorption maxima of all mutants were blue shifted with an increase in the Cl^- concentration. The dissociation constants were 5, 89, 153, and 159 mM for the wild-type *p*hR, and S130A, S130T, and S130C mutants, respectively, at pH 7.0 and 25°C. In the case of T126V, the apparent half-maximal binding concentration was 32 mM, the order being wild-type < T126V < S130A < S130C and S130T (Table 1).

Photocycle of the Wild-Type phR and Ser130 Mutants in the Presence of Chloride—The wild-type *p*hR and $Ser130^{phR}$ mutants solubilized with DM were excited by a laser flash in 1 M NaCl. Figure 3 shows the flash-induced light-dark difference spectra, logarithmic time scale, measured between 350 and 750 nm. Since the binding of Cl^- is described with a K_d of 5 mM for the wild-type *p*hR and 90–160 mM for the S130 mutants, no photoproducts derived from a Cl^- free form are present at the Cl^- concentration of 1 M. The scattered laser flash caused a strong artifact at the beginning of the trace within 10 μs, thus the optical data could be evaluated reliably after 10 μs. The data obtained for the wild-type *p*hR are essentially the same as those reported previously (*18*, *24*, *27*, *28*).

Table 1. **Dissociation constants (K_d), absorption maxima (λ_{max}) and differences in absorption maxima between Cl^- free and Cl^- bound forms of the wild-type *p*hR, and T126 and S130 mutants of *p*hR at pH 7.0 and 25°C.**

Proteins	K_d (mM)	λ_{max}		Difference (nm)
		not present	1 M NaCl	
Wild type[a]	5	599	577	22
T126V	32	584	567	17
S130A[a]	89	611	581	30
S130C[a]	159	600	577	23
S130T[a]	153	588	572	16

The dissociation constant was determined by least-square fitting.
[a]Reference values (*20*).

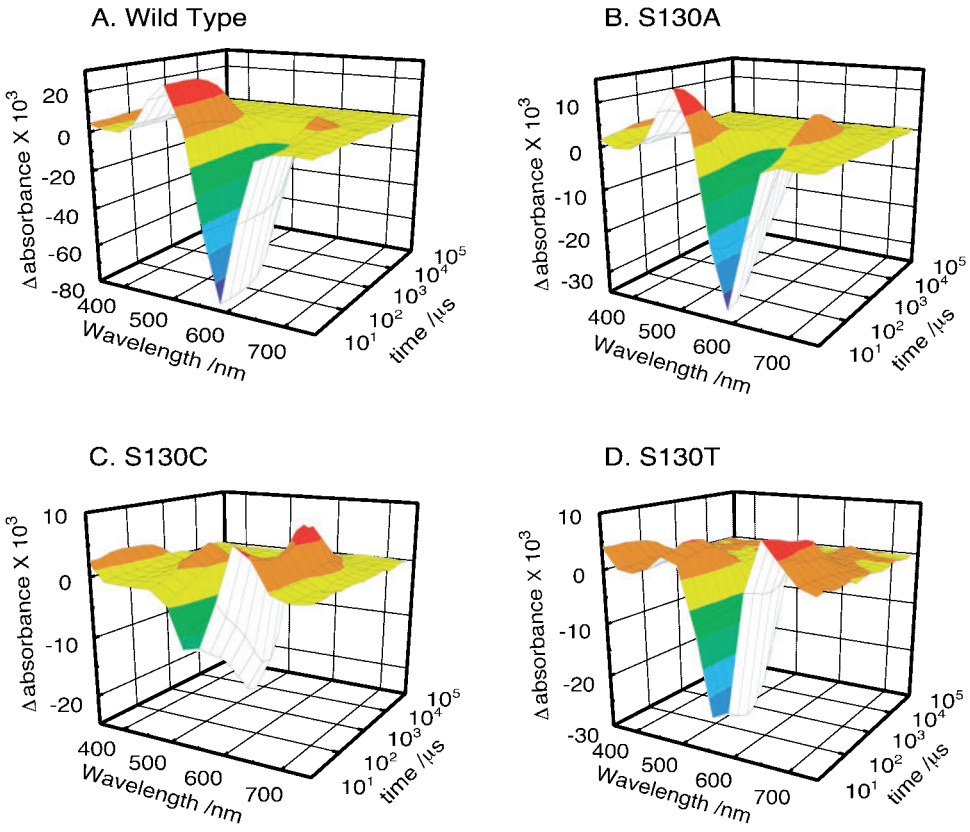

Fig. 3. **Differential transient spectra of the wild-type *p*hR (A), and Ser-130 mutants S130A (B), S130C (C), and S130T (D).** Proteins were solubilized in 10 mM MOPS (pH 7.0) containing 0.1% DM and 1 M NaCl. The measurements were carried out at 20°C. Data plots for a respective measuring wavelength were originally obtained as 125,893 linear points and were reduced to 378 points by converting to a logarithmic time scale from 10 μs to 100 ms. The traces were measured from 350 to 750 nm with a resolution of 10 nm (41 spectral points).

Kinetic analysis of these time-dependent spectral shifts was performed using a method known as singular value decomposition (SVD) (*26*, *29*) in order to determine the number of singular values which represent the original data matrix sufficiently. On this analysis, it was found that three singular values represent a sufficient matrix for the wild-type *p*hR and S130 mutants. Including additional singular values added noise to the data without changing the results of further analysis. The global fitting of the time-dependent spectral shifts between 10 μs and 100 ms, using three "apparent" time constants for the wild-type *p*hR and S130 mutants, gave adequate fits to the data (see Fig. 4 for examples). Table 2 and Fig. 5 show the apparent time constants and spectral amplitudes associated with the apparent time constants (called B-spectra, hereafter).

The photocycle of *p*hR has been studied extensively (*16*, *18*), and the scheme was reported to be $p\mathrm{hR}_{578} \rightarrow \mathrm{K}_{600} \leftrightarrow \mathrm{L}_{520} \leftrightarrow \mathrm{N} \leftrightarrow \mathrm{O}_{640} \leftrightarrow p\mathrm{hR}' \rightarrow p\mathrm{hR}_{578}$ (*16*), where the numbers represent the l_{max} of the respective species. The release and uptake of Cl^- are associated with the N to O and O to hR′ reactions, respectively. In Figure 5, the peaks calculated according to results of the singular value decomposition were assigned sequentially to the K, L, and O intermediates for the wild-type *p*hR, S130C, and S130T (except for S130A; see later). The three kinds of apparent time constants attributed to τ_1(K → L), τ_2(L → O), and τ_3(O → hR) are listed in Table 2, and the corresponding B-spectra are shown in Fig. 5 as the curves of – – – (K → L), —— (L → O), and - - - - (O → hR), respectively. Figure 4A shows the absorbance changes of the wild-type *p*hR after the flash against time on a logarith-

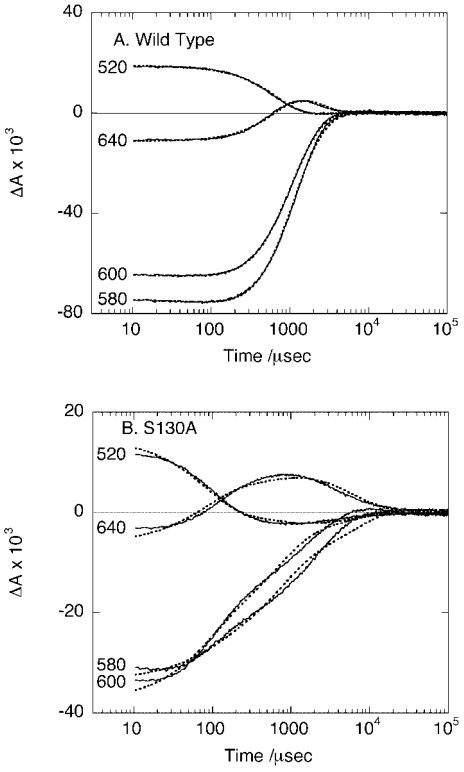

Fig. 4. **Traces of the transient absorption change after photoexcitation of the wild-type *p*hR (A) and S130A mutant (B).** The time courses are shown for selected wavelengths only (520, 580, 600, and 640 nm). The dotted lines represent the result of global fitting using three exponents.

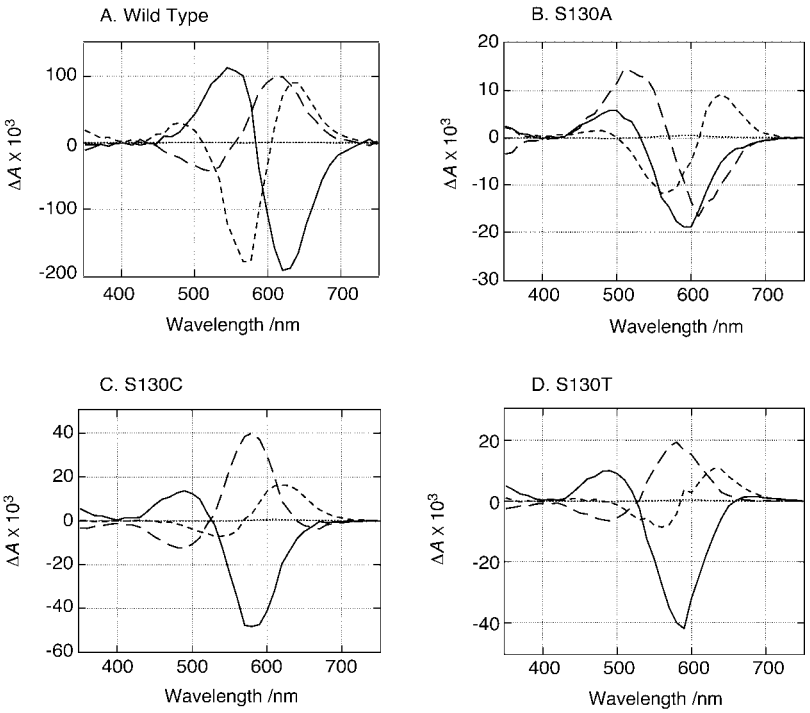

Fig. 5. **Results of singular value decomposition and global fitting of a data set recorded between 10 μs and 100 ms.** The data for the wild-type *p*hR (A) and Ser-130 mutants (B, S130A; C, S130C; D, S130T) were fitted with a three-exponential equation. Spectral amplitudes are associated with the following apparent lifetimes listed in Table 2: – – –, τ_1; ——, τ_2; - - - -, τ_3; ·····, $\tau_4 = \infty$. All samples were suspended in 10 mM MOPS (pH 7.0) containing 0.1% DM and 1 M NaCl.

mic scale. This shows the increase in the 520-nm band (due to L) within 10 μs, while the SVD analysis gave a τ_1 of 237 μs, which was assumed to be the time constant of the K→L process judging from the λ_{max} of the B-spectra in Fig. 5. These findings seem contradictory but they reveal the presence of a reverse reaction from L to K; when the respective rate constants are denoted as $k_{(K\rightarrow L)}$, $k_{(L\rightarrow K)}$, and $k_{(L\rightarrow O)}$, we assume that $k_{(K\rightarrow L)} > k_{(L\rightarrow K)} \gg k_{(L\rightarrow O)}$, as was also shown by Váró *et al* (*18*). Under these conditions, SVD analysis may give the overall slow transition of K to L. Thus, the time constant of τ_1 does not exactly express $k_{(K\rightarrow L)}$ only. The spectra of the wild-type *p*hR in Fig. 5 indicate that at the transition of τ_3 (shown by - - - -), *i.e.*, at the recovery of *p*hR, the spectrum has two positive bands, from whose λ_{max} they are attributed to L and O intermediates. This might suggest that equilibrium between L and O should be considered for the detailed analysis of the wild-type *p*hR, as shown by previous studies (*18*).

We also determined that S130A had three spectral components, based on the results of SVD analysis. The B-spectra shown in Figure 5 may not contain that of the K-intermediate, and the absorbance depletion at 600 nm was a little greater than that of 580 nm at several microseconds after the flash (see Fig. 4B). If the K-intermediate exists in this time range, ΔA_{600} should be smaller (that is, it should be more positively deflected) than ΔA_{580} because K is located at a longer wavelength than the depleted original pigment. These imply the very fast decay of K and the lack of the reverse reaction from L to K, unlike in the case of the wild-type *p*hR. Thus, a different model is needed to explain the scheme of S130A (see "DISCUSSION").

Table 2. **Apparent time constants of the photocycle of the wild-type *p*hR, and T126 and S130 mutants of *p*hR.**

Proteins	τ_1/μs	τ_2 μs	τ_2'/μs	τ_3/μs
Wild type	237	368	–	563
T126V	390	664	–	1,715
S130A	–	56	473	4,356
S130C	206	752	–	2,896
S130T	50	254	–	927

Proteins were solubilized in 10 mM MOPS (pH 7.0) containing 0.1% DM and 1 M NaCl. The measurements were carried out at 20°C. The meaning of apparent time constants (τ_i) is discussed in the text and shown in Fig. 7.

For S130C and S130T, the B-spectra show a photocycling scheme similar to that of the wild-type *p*hR, but the time constants of the respective steps are different. Note that the B-spectra are a function of the kinetic constants involved in the transition step. It is interesting that the S130C mutant has a prominent O-intermediate (Fig. 3C), a feature that awaits further investigation.

Photocycle of the T126V Mutant in the Presence of Chloride—The T126V mutant solubilized with DM was also excited by a laser flash in 1 M NaCl. Figure 6 shows the flash-induced light-dark difference spectra in the presence of chloride. Table 2 and Figure 6 show the apparent time constants and spectral amplitudes associated with the apparent time constants. B-spectra of the T126V mutant show a photocycling scheme similar to that of the wild-type *p*hR, but the time constants of respective steps are larger than those of the wild-type *p*hR.

DISCUSSION

Chloride Ion Binding Of S130 And T126V Mutants Of Phr—In the present study, we examined the roles and functions of $Thr126^{phR}$ (the site homologous to $Thr111^{shR}$) and $Ser130^{phR}$ (the site homologous to $Ser115^{shR}$). The apparent dissociation constants (K_d) of a chloride ion increased in the order of the wild-type < T126V < S130A

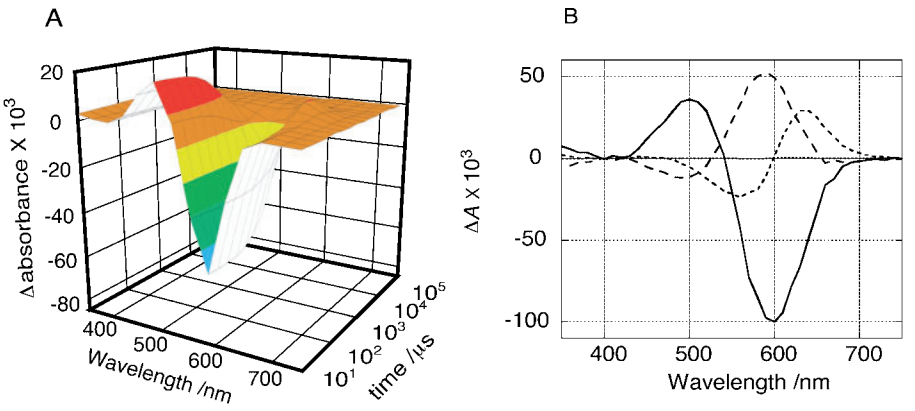

Fig. 6. **Differential transient spectrum (A), and the result of singular value decomposition and global fitting of a data set recorded between 10 μs and 100 ms (B) of the T126V mutant.** Proteins were solubilized in 10 mM MOPS (pH 7.0) containing 0.1% DM and 1 M NaCl. The measurement conditions and line styles are the same as those shown in Fig. 3 and 5, respectively.

< S130C and S130T, as listed in Table 1. For the T111V mutation of *s*hR, a similar increasing in the K_d value has been observed (*9*). However, there has been no report on the S115 mutation of *s*hR. The findings in the present study indicate that the influence of the T126^{phR} mutation on the chloride affinity is smaller than that of S130^{phR}. In the crystal structure of *s*hR (*6*), the nearest amino acid residues to the chloride ion that interact with the retinal Schiff base are T111 and S115 in the C helix (Fig. 1). Although both residues have an OH group, only the OH of S115 residue faces the chloride. The hydroxyl oxygen of S115 is located 3.1 Å from the chloride ion and 3.8 Å from the nitrogen of the Schiff base. In addition, Ser115, which is homologous to Thr89^{bR}, and may participate in the 'switch of the pump' (*30*) and color regulation (*31*), is conserved in all known sequences of hRs (*32*). Thus, it is strongly suggested that Ser130^{phR} is an essential residue that participates directly the chloride ion transfer or switching, and that interacts indirectly with other residues in the retinal-binding pocket.

Photocycle of phR, and the Kinetic Effects of S130 and T126 Mutants—The photocycle of S130 mutants except for S130A and that of the T126V mutant followed a similar scheme to that of the wild-type *p*hR, as mentioned in the results section. Thus, the photocycles of the wild-type *p*hR, S130C, S130T and T126V mutants can be modeled adequately with an unbranched kinetic scheme, as depicted in Fig. 7A. In the case of *s*hR, the T111V mutant was only an additional participant of the binding site (*9*), but in the case of the T126V mutant of *p*hR, the apparent time constant, particularly during the uptake and

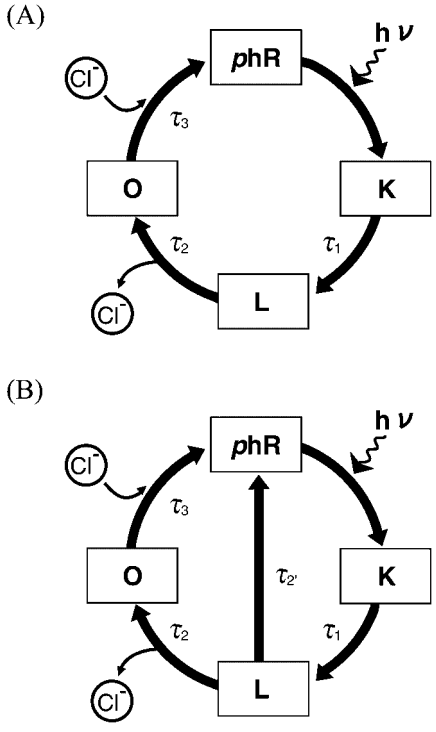

Fig. 7. **Photocycle schemes of *p*hRs simplified to fit the data.** (A) Sequential cycle for the wild-type *p*hR, S130C, S130T, and T126V, and (B) the branched cycle for S130A. Apparent time constants of the photocycle (τ_i) are shown.

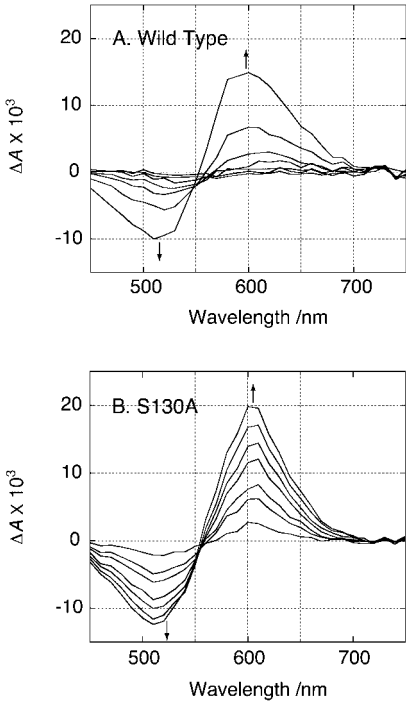

Fig. 8. **Transient absorption difference spectra of the wild type *p*hR (A) and S130A mutant (B).** The baseline was taken at 30 μs after the flash. Representative spectra (50, 80, 100, 152, 200, 300, 540 μs) are shown. Arrows indicate spectral changes with increasing time.

release step, become slightly slower than that of wild type.

In the case of the S130A mutant, the photocycle is drastically changed. The formation and decay of the K intermediate occurred too quickly to be detected, and no equilibrium existed between K and L. The reason for the lack of equilibrium should be clarified on a molecular basis in the future. Regarding the decay of the L intermediate, we were unable to assign a linear sequence of intermediates because two positive peaks (ΔA in Fig. 5B) around 520 nm appeared at different τ values. It may be that one represents the L $\rightarrow$ O reaction (τ_2) and the other the L $\rightarrow$ hR reaction (τ_2'), based on the absorption maxima of the B-spectra (Fig. 5B). Figure 8 shows the branching process of S130A. The baseline is taken at 30 μs after the flash in this figure, where the depletion of a 520-nm band (contributed by L) is observed with the appearance of a concomitant band at a longer wavelength (Fig. 8B). It is noteworthy that the wavelength of this positive band does not change during the observation time (50–540 μs). Furthermore, an isosbestic point (not exactly but approximately) appears. If this branching process is accepted, these observations are easy to interprete. On the other hand, a similar plot for the wild-type *p*hR (Fig. 8A) shows a gradual shift in the absorption maximum of the positive band, which corresponds well to the transfer to O and subsequent *p*hR.

The branched pathways L $\rightarrow$ O and L$\rightarrow$ hR only appear in the case of the S130A mutant. In addition, Table 2 indicates that the apparent time constant τ_2 of S130A corresponding to the L $\rightarrow$ O reaction decreases considerably compared with in the case of other proteins that have an OH or SH group at the side chain of position 130. The lack of a residue capable of forming a hydrogen bond is predicted to affect the L $\rightarrow$ O reaction drastically. This suggests that the effective switching of the chloride accessibility between the extracellular and cytoplasmic chloride binding sites next to the Schiff base is facilitated by the hydrogen bond of Ser130^{phR} with the chloride ion. From the results of a Fourier transform infrared (FTIR) study of *s*hR, the presence of two L intermediates, L_a and L_b, was recently proposed, in which the structure of the protein and internal water molecules are different but chloride stays at the same site close to the Schiff base (*33*). In addition, at a very high chloride concentration (>5 M), similar branching of the photocycle from L (latter of L) directly back to the dark state of *p*hR has been proposed, although the destabilization effect on the protein structure of a high salt concentration could not be completely eliminated (*34*). These reports support our finding that a branched pathway from the L intermediate is observed on the substitution of the putative switching site, Ser130^{phR}, with Ala, a hydrogen-bonding disabled residue. A more detailed study is needed so that we can understand the change in chloride accessibility from the structural basis of *p*hR and the hydrogen bonding efficiency for the OH/SH groups at the Ser130 sites, including bound water molecules.

CONCLUSION

The wild-type *p*hR, and Ser130 or Thr126 mutants with Thr, Cys, Ala, or Val substituted, respectively, exhibited various degrees of chloride accessibility. The photocycles of the wild-type *p*hR, and T126V, S130C, and S130T mutants of *p*hR contained the typical photointermediates in series, although the reaction rates were different. On the contrary, the photocycle of the S130A mutant was quite different, and we analyzed the branched pathway from L to hR or L to O. Our results indicate that the Ser residue of *p*hR at position 130, which may be in contact with the chloride ion directly in the retinal pocket, is one of the essential residues for chloride binding and the transport/switch mechanism.

The authors are very grateful to Dr. Y. Imamoto, Dr. M. Iwamoto and Y. Sudo for the invaluable discussions and advice.

REFERENCES

1. Booth, P.J., Templer, R.H., Curran, A.R., and Allen, S.J. (2001) Can we identify the forces that drive the folding of integral membrane proteins? *Biochem. Soc. Trans* **29**, 408–413
2. Váró, G. (2000) Analogies between halorhodopsin and bacteriorhodopsin. *Biophys. Biochem. Acta* **1460**, 220–229
3. Lanyi, J.K. (1997) Mechanism of ion transport across membranes. Bacteriorhodopsin as a prototype for proton pumps. *J. Biol. Chem.* **272**, 31209–31212
4. Lozier, R.H., Bogomolni, R.A., and Stoeckenius, W. (1975) Bacteriorhodopsin: a light-driven proton pump in *Halobacterium Halobium*. *Biophys. J.* **15**, 955–962
5. Luecke, H., Schobert, B., Richter, H.T., Cartailler, J.P., and Lanyi, J.K. (1999) Structure of bacteriorhodopsin at 1.55 Å resolution. *J. Mol. Biol.* **291**, 899–911
6. Kolbe, M., Besir, H., Essen, L.O., and Oesterhelt, D. (2000) Structure of the light-driven chloride pump halorhodopsin at 1.8 Å resolution. *Science* **288**, 1390–1396
7. Pebay-Peyroula, E., Rummel, G., Rosenbusch, J.P., and Landau, E.M. (1997) X-ray structure of bacteriorhodopsin at 2.5 angstroms from microcrystals grown in lipidic cubic phases. *Science* **277**, 1676–1681
8. Royant, A., Nollert, P., Edman, K., Neutze, R., Landau, E.M., Pebay-Peyroula, E., and Navarro, J. (2001) X-ray structure of sensory rhodopsin II at 2.1-A resolution. *Proc. Natl Acad. Sci. USA* **98**, 10131–10136
9. Rüdiger, M. and Oesterhelt, D. (1997) Specific arginine and threonine residues control anion binding and transport in the light-driven chloride pump halorhodopsin. *EMBO J.* **16**, 3813–3821
10. Otomo, J., Tomioka, H., and Sasabe, H. (1992) Properties and the primary structure of a new halorhodopsin from halobacterial strain *mex*. *Biochim. Biophys Acta* **1112**, 7–13
11. Soppa, J., Duschl, J., and Oesterhelt, D. (1993) Bacterioopsin, haloopsin, and sensory opsin I of the halobacterial isolate *Halobacterium sp*. strain SG1: three new members of a growing family. *J. Bacteriol.* **175**, 2720–2726
12. Ihara, K., Umemura, T., Katagiri, I., Kitajima-Ihara, T., Sugiyama, Y., Kimura, Y., and Mukohata, Y. (1999) Evolution of the archaeal rhodopsins: evolution rate changes by gene duplication and functional differentiation. *J. Mol. Biol.* **285**, 163–174
13. Ng, W.-V., Kennedy, S.P., Mahairas, G.G., Berquist, B., Pan, M., Shukla, H.D., Lasky, S.R., Baliga, N.S., Thorsson, V., Sbrogna, J., Swartzell, S., Weir, D., Hall, J., Dahl, T.A., Welti, R., Goo, Y.A., Leithauser, B., Keller, K., Cruz, R., Danson, M.J., Hough, D.W., Maddocks, D.G., Jablonski, P.E., Krebs, M.P., Angevine, C.M., Dale, H., Isenbarger, T.A., Peck, R.F., Pohlschroder, M., Spudich, J.L., Jung, K.W., Alam, M., Freitas, T., Hou, S., Daniels, C.J., Dennis, P.P., Omer, A.D., Ebhardt, H., Lowe, T.M., Liang, P., Riley, M., Hood, L., and DasSarma, S. (2000) Genome sequence of Halobacterium species NRC-1. *Proc. Natl Acad. Sci. USA* **97**, 12176–12181
14. Lanyi, J.K. (1990) Halorhodopsin, a light-driven electrogenic chloride-transport system. *Physiol. Rev.* **70**, 319–330

15. Matsuno-Yagi, A. and Mukohata, Y. (1980) ATP synthesis linked to light-dependent proton uptake in a rad mutant strain of *Halobacterium* lacking bacteriorhodopsin. *Arch. Biochem. Biophys.* **199**, 297–303
16. Váró, G., Needleman, R., and Lanyi, J.K. (1995a) Light-driven chloride ion transport by halorhodopsin from *Natronobacterium pharaonis*. 2. Chloride release and uptake, protein conformation change, and thermodynamics. *Biochemistry* **34**, 14500–14507
17. Bivin, D.B. and Stoeckenius, W. (1986) Photoactive retinal pigments in haloalkaliphilic bacteria. *J. Gen. Microbiol.* **132**, 2167–2177
18. Váró, G., Brown, L.S., Sasaki, H., Kandori, H., Maeda, A., Needleman, R., and Lanyi, J.K. (1995c) Light-driven chloride ion transport by halorhodopsin from *Natronobacterium pharaonis*. 1. The photochemical cycle. *Biochemistry* **34**, 14490–14499
19. Duschl, A., Lanyi, J.K., and Zimányi, L. (1990) Properties and photochemistry of a halorhodopsin from the haloalkalophile, *Natronobacterium pharaonis*. *J. Biol. Chem.* **265**, 1261–1267
20. Sato, M., Kikukawa, T., Araiso, T., Okita, H., Shimono, K., Kamo, N., Demura, M., and Nitta, K. (2003) Ser-130 of *Natronobacterium pharaonis* halorhodopsin is important for the chloride binding. *Biophys. Chem.* in press
21. Váró, G., Zimányi, L., Fan, X., Sun, L., Needleman, R., and Lanyi, J.K. (1995b) Photocycle of halorhodopsin from *Halobacterium salinarium*. *Biophys. J.* **68**, 2062–2072
22. Sato, M., Kanamori, T., Kamo, N., Demura, M., and Nitta, K. (2002) Stopped-flow analysis on anion binding to blue-form halorhodopsin from *Natronobacterium pharaonis*: comparison with the anion-uptake process during the photocycle. *Biochemistry* **41**, 2452–2458
23. Shimono, K., Iwamoto, M., Sumi, M., and Kamo, N. (1997) Functional expression of pharaonis phoborhodopsin in *Escherichia coli*. *FEBS Lett.* **420**, 54–56
24. Hohenfeld, I.P., Wegener, A.A., and Engelhard, M. (1999) Purification of histidine tagged bacteriorhodopsin, *pharaonis* halorhodopsin and *pharaonis* sensory rhodopsin II functionally expressed in *Escherichia coli*. *FEBS Lett.* **442**, 198–202
25. Takao, K., Kikukawa, T., Araiso, T., and Kamo, N. (1998) Azide accelerates the decay of M-intermediate of *pharaonis phoborhodopsin*. *Biophys. Chem.* **73**, 145–154
26. Henry, E.R. and Hofrichter, J. (1992) Singular value decomposition: application to analysis of experimental data. *Methods Enzymol.* **210**, 129–193
27. Scharf, B. and Engelhard, M. (1994) Blue halorhodopsin from *Natronobacterium pharaonis*: wavelength regulation by anions. *Biochemistry* **33**, 6387–6393
28. Ludmann, K., Ibron, G., Lanyi, J.K., and Váró, G. (2000) Charge motions during the photocycle of *pharaonis* halorhodopsin. *Biophys. J.* **78**, 959–966
29. Hendler, R.H. and Shrager, R.I. (1994)_Deconvolutions based on singular value decomposition and the pseudoinverse: a guide for beginners. *J. Biochem. Biophys. Methods* **28**, 1–33
30. Kandori, H., Yamazaki, Y., Shichida, Y., Raap, J., Lugtenburg, J., Belendky, M., and Herzfeld, J. (2001) Tight Asp-85–Thr-89 association during the pump switch of bacteriorhodopsin. *Proc. Natl Acad. Sci. USA* **98**, 1571–1576
31. Russell, T.S., Coleman, M., Rath, P., Nilsson, A., and Rothschild, K.J. (1997) Threonine-89 participates in the active site of bacteriorhodopsin: evidence for a role in color regulation and Schiff base proton transfer. *Biochemistry* **36**, 7490–7497
32. Oesterhelt, D. (1995) Structure and function of halorhodopsin. *Isr. J. Chem.* **35**, 475–494
33. Chon, Y. –S., Kandori, H., Sasaki, J., Lanyi, J.K., Needleman, R., and Maeda, A. (1999) Existence of two L photointermediates of halorhodopsin from *Halobacterium salinarium*, differing in their protein and water FTIR bands. *Biochemistry* **38**, 9449–9455
34. Hackmann, C., Guijarro, J., Chizhov, I., Engelhard, M., Rodig, C., Siebert, F. (2001) Static and time-resolved step-scan Fourier transform infrared investigations of the photoreaction of halorhodopsin from *Natronobacterium pharaonis*: consequences for models of the anion translocation mechanism. *Biophys. J.* **81**, 394–406